J|A|C|S
ARTICLES
Published on Web 12/03/2004

The Mobile Proton in Polyalanine Peptides

Motoya Kohtani, Jean E. Schneider, Thaddeus C. Jones, and Martin F. Jarrold*

Contribution from the Department of Chemistry, Indiana University, 800 East Kirkwood Avenue, Bloomington, Indiana 47405-7102

Received August 3, 2004; E-mail: mfj@indiana.edu

Abstract: Ion mobility measurements have been performed for protonated polyalanine peptides ($A_{10} + H^+$, $A_{15} + H^+$, $A_{20} + H^+$, $A_{25} + H^+$, and $A_{15}NH_2 + H^+$) as a function of temperature using a new high-temperature drift tube. Peaks due to helices and globules were found at room temperature for all peptides, except for $A_{10} + H^+$ (where only the globule is present). As the temperature is increased, the helix and globule peaks broaden and merge to give a single narrow peak. This indicates that the two conformations interconvert rapidly at elevated temperatures. The positions of the merged peaks show that $A_{15} + H^+$ and $A_{15}NH_2 + H^+$ spend most of their time as globules when heated, while $A_{20} + H^+$ and $A_{25} + H^+$ spend most of their time as helices. The helix/globule transitions are almost certainly accompanied by intramolecular proton transfer, and so, these results suggest that the proton becomes mobile (able to migrate freely along the backbone) at around 450 K. The peptides dissociate as the temperature is increased further to give predominantly the b_n^+, b_{n-1}^+, b_{n-2}^+, ... series of fragment ions. There is a correlation between the ease of fragmentation and the time spent in the helical conformation for the $A_n + H^+$ peptides. Helix formation promotes dissociation because it pools the proton at the C-terminus where it is required for dissociation to give the observed products. In addition to the helix and globule, an antiparallel helical dimer is observed for the larger peptides. The dimer can be collisionally dissociated by injection into the drift tube at elevated kinetic energies.

Introduction

Intramolecular proton transfer in ionized peptides has received a lot of attention recently. The majority of these studies have examined the role of the so-called "mobile proton" in explaining peptide fragmentation patterns observed in mass spectrometry studies.[1−9] When excited under low energy conditions, protonated peptides fragment predominantly by charge-directed reactions. To account for the observed fragmentation patterns, it is necessary to assume the proton is not sequestered at basic sites, but that it is free to migrate before dissociation occurs. Over the years, evidence supporting this proposal has steadily increased. Extensive H/D mixing in the fragmentation of both metastable and collisionally activated amino acids further supports the mobile proton interpretation.[10,11] Theoretical investigations of potential fragmentation pathways have also been fruitful, especially in evaluating the possible protonation sites along the peptide backbone.[12−17]

In contrast, studies of the conformations of unsolvated peptides have usually been performed at or near room temperature.[18−22] Ion mobility measurements have proven to be especially adept at differentiating geometrical isomers of peptides, the most important species for protonated peptides with more than a few residues are the helix and the globule (a compact random-looking three-dimensional structure).[23,24] Through these studies, we have found that when the charge is localized

(1) Johnson, R. S.; Martin, S. A.; Biemann, K. *Int. J. Mass Spectrom. Ion Processes* **1988**, *86*, 137−154.
(2) Burlet, O.; Orkiszewski, R. S.; Ballard, K. D.; Gaskell, S. J. *Rapid Commun. Mass Spectrom.* **1992**, *6*, 658−662.
(3) McCormack, A. L.; Somogyi, A.; Dongré, A. R.; Wysocki, V. H. *Anal. Chem.* **1993**, *65*, 2859−2872.
(4) Jones, J. L.; Dongré, A. R.; Somogyi, A.; Wysocki, V. H. *J. Am. Chem. Soc.* **1994**, *116*, 8368−8369.
(5) Cox, K. A.; Gaskell, S. J.; Morris, M.; Whiting, A. *J. Am. Soc. Mass Spectrom.* **1996**, *7*, 522−531.
(6) Dongré, A. R.; Jones, J. L.; Somogyi, A.; Wysocki, V. H. *J. Am. Chem. Soc.* **1996**, *118*, 8365−8374.
(7) Nair, H.; Wysocki, V. H. *Int. J. Mass Spectrom. Ion Processes* **1998**, *174*, 95−100.
(8) Vaisar, T.; Urban, Y. *J. Mass Spectrom.* **1998**, *33*, 505−524.
(9) Wysocki, V. H.; Tsaprailis, G.; Smith, L. L.; Breci, L. A. *J. Mass Spectrom.* **2000**, *35*, 1399−1406.
(10) Harrison, A. G.; Yalcin, T. *Int. J. Mass Spectrom.* **1997**, *165−166*, 339−347.
(11) Demmers, J. A.; Rijkers, D. T. S.; Haverkamp, J.; Killian, J. A.; Heck, A. J. R. *J. Am. Chem. Soc.* **2002**, *124*, 11191−11198.
(12) Klassen, J. S.; Kebarle, P. *J. Am. Chem. Soc.* **1997**, *119*, 6552−6563.
(13) Csonka, I. P.; Paizs, B.; Lendvay, G.; Suhai, S. *Rapid Commun. Mass Spectrom.* **2000**, *14*, 417−431.
(14) Rogalewicz, F.; Hoppilliard, Y. *Int. J. Mass Spectrom.* **2000**, *199*, 235−252.
(15) Paizs, B.; Csonka, I. P.; Lendvay, G.; Suhai, S. *Rapid Commun. Mass Spectrom.* **2001**, *15*, 637−650.
(16) Rodriquez, C. F.; Cunje, A.; Shoeib, T.; Chu, I. K.; Hopkinson, A. C.; Siu, K. W. M. *J. Am. Chem. Soc.* **2001**, *123*, 3006−3012.
(17) El Aribi, H.; Rodriquez, C. F.; Almeida, D. R. P.; Ling, Y.; Mak, W. W.-N.; Hopkinson, A. C.; Siu, K. W. M. *J. Am. Chem. Soc.* **2003**, *125*, 9229−9236.
(18) Wyttenbach, T.; Bushnell, J. E.; Bowers, M. T. *J. Am. Chem. Soc.* **1998**, *120*, 5098−5103.
(19) Hudgins, R. R.; Mao, Y.; Ratner, M. A.; Jarrold, M. F. *Biophys. J.* **1999**, *76*, 1591−1597.
(20) Taraszka, J. A.; Li, J. W.; Clemmer, D. E. *J. Phys. Chem. B* **2000**, *104*, 4545−4551.
(21) Counterman, A. E.; Clemmer, D. E. *J. Am. Chem. Soc.* **2001**, *123*, 1490−1498.
(22) Ruotolo, B. T.; Verbeck, G. F.; Thomson, L. M.; Gillig, K. J.; Russell, D. H. *J. Am. Chem. Soc.* **2002**, *124*, 4214−4215.
(23) Hudgins, R. R.; Ratner, M. A.; Jarrold, M. F. *J. Am. Chem. Soc.* **1998**, *120*, 12974−12975.
(24) Hudgins, R. R.; Jarrold, M. F. *J. Am. Chem. Soc.* **1999**, *121*, 3494−3501.

at the C-terminus, polyalanine peptides (and other peptides based on amino acids with nonpolar side chains) are usually helical. The helix is stabilized by favorable interactions between the charge and the helix macrodipole. On the other hand, placing the charge at the N-terminus collapses the helix into a compact globule.[25−28]

Here, we report high-temperature ion mobility measurements for polyalanine peptides aimed at examining conformational changes up to the point where the peptides dissociate. These studies provide a link between the conformational studies that are normally performed close to room temperature and the fragmentation studies that require more elevated internal energies. In the studies described here, we have examined the conformations of several polyalanine peptides over a broad temperature range, from room temperature up to the point where the peptides are almost entirely dissociated. Both helical and globular conformations are found at room temperature for the larger polyalanine peptides studied here ($Ala_{15} + H^+$, $Ala_{20} + H^+$, and $Ala_{25} + H^+$). For $Ala_{15} + H^+$, the helix converts into a globule as the temperature is increased, while $Ala_{20} + H^+$ and $Ala_{25} + H^+$ convert into a state that is intermediate between the helix and globule and involves rapid interconversion between these two geometries. Since these helix/globule transitions almost certainly involve proton transfer, the rapid structural changes are an indicator for the emergence of the mobile proton state, where the proton can migrate freely along the peptide backbone.

In the studies described here, the conformations of the peptides are probed (as a function of temperature) using ion mobility measurements.[29,30] The mobility of an ion is a measure of how rapidly it moves through a buffer gas under the influence of a weak electric field. The mobility depends on the average collision cross section; ions with small compact geometries have fewer collisions and travel more rapidly through the buffer gas. Geometries are assigned by comparing the measured cross sections to average cross sections calculated for trial geometries, which are usually derived from molecular dynamics simulations. In the present work, the cross sections are calculated using MOBCAL,[31] which correctly accounts for multiple scattering events and the long-range interactions between the ion and the buffer gas.[32,33]

Experimental Section

A schematic diagram of the experimental apparatus is shown in Figure 1. The apparatus is similar to that described previously,[28] except that it is equipped with a high-temperature drift tube, which is described in more detail below. Ions produced by electrospray enter the apparatus through a heated capillary interface maintained at 135−145 °C; they pass through a differentially pumped region and are then focused into the drift tube through an electrostatic shutter. The shutter can be pulsed to permit short (100 μs) packets of ions to enter the drift tube. The ions travel across the drift tube under the influence of a weak electric field and exit through a small aperture. The ions that exit are focused into a quadrupole mass spectrometer, where they are mass analyzed. The mass-analyzed ions are then detected with an off-axis collision dynode and a pair of microchannel plates. Short packets of ions are allowed to enter the drift tube, and their arrival time distribution at the detector is recorded using a multichannel scaler that is synchronized with the ion shutter. Drift times are determined from the arrival time distributions by subtracting the time the ions spend traveling outside of the drift tube. The measured drift times are converted into collision cross sections using[34]

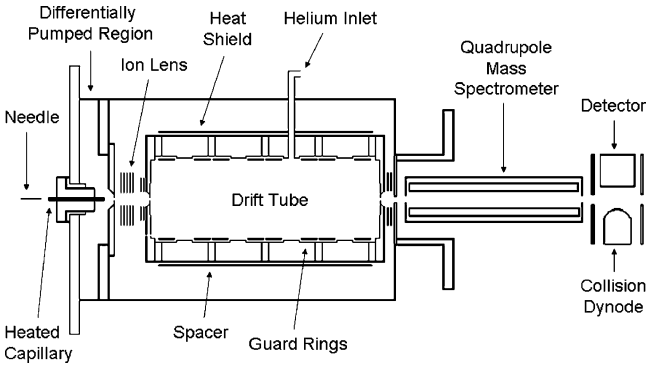

Figure 1. Schematic diagram of the experimental apparatus showing the new high-temperature drift tube.

$$\Omega_{avg}^{(1,1)} = \frac{(18\pi)^{1/2}}{16}\left[\frac{1}{m} + \frac{1}{m_b}\right]^{1/2}\frac{ze}{(k_B T)^{1/2}}\frac{t_D E}{L\rho} \qquad (1)$$

where m and m_b are the masses of the ion and buffer gas, respectively, and ze is the charge; t_D is the drift time, E the drift field, and ρ the buffer gas number density.

The high-temperature drift tube was designed to operate at up to ~800 °C (1100 K). It is 30.78 cm long and consists of four cylindrical sections and two end plates made of stainless steel. The drift tube is equipped with heat shields to reduce radiative cooling at high temperatures. The end plates and cylindrical sections are heated by separate Thermocoax heaters that are embedded in a way that minimizes magnetic fields on the drift tube axis. The temperature of each end plate and each section is individually regulated to within 1 °C by a microprocessor-based temperature controller. Stainless steel spacers coated on both sides with 0.001 in. thick alumina serve to electrically isolate the end plates and cylindrical sections. Each cylindrical section has two guard rings to ensure a uniform electric field along the axis of the drift tube. The guard rings, the cylindrical sections, and the end plates are connected to an external voltage divider. The drift voltage is usually 180−380 V, with a helium buffer pressure of ~3 Torr at room temperature. These conditions fulfill the low-field criterion,[34] thus the measured ion mobility is not affected by field effects (i.e., the ions are not aligned with the field). The resolving power of the high-temperature drift tube described here is equivalent to that of the low-temperature version used previously when operated under the same conditions.[28] However, the resolving power (which is limited by diffusion) scales with $T^{-1/2}$, and so it systematically degrades as the temperature is increased.

The peptides (A_{10}, A_{15}, A_{20}, A_{25}, and $A_{15}NH_2$) were synthesized using FastMoc chemistry on an Applied Biosystems 433A peptide synthesizer. After synthesis, the peptides were cleaved from the HMP resin using a 95% TFA and 5% water (v/v) mixture, precipitated using cold diethyl ether, and lyophilized. The peptides were used without further purification. Electrospray solutions were prepared by dissolving 1 mg of peptide in 1 mL of TFA and 0.1 mL of purified water and electrosprayed

(25) Kinnear, B. S.; Jarrold, M. F. *J. Am. Chem. Soc.* **2001**, *123*, 7907−7908.
(26) Kohtani, M.; Kinnear, B. S.; Jarrold, M. F. *J. Am. Chem. Soc.* **2000**, *122*, 12377−12378.
(27) Kinnear, B. S.; Kaleta, D. T.; Kohtani, M.; Hudgins, R. R.; Jarrold, M. F. *J. Am. Chem. Soc.* **2000**, *122*, 9243−9256.
(28) Kinnear, B. S.; Hartings, M. R.; Jarrold, M. F. *J. Am. Chem. Soc.* **2001**, *123*, 5660−5667.
(29) Clemmer, D. E.; Jarrold, M. F. *J. Mass Spectrom.* **1997**, *32*, 577−592.
(30) Wyttenbach, T.; Bowers, M. T. *Top. Curr. Chem.* **2003**, *225*, 207−232.
(31) MOBCAL is available from our web site at http://nano.chem.indiana.edu.
(32) Mesleh, M. F.; Hunter, J. M.; Shvartsburg, A. A.; Schatz, G. C.; Jarrold, M. F. *J. Phys. Chem.* **1996**, *100*, 16082−16086.
(33) Shvartsburg, A. A.; Jarrold, M. F. *Chem. Phys. Lett.* **1996**, *261*, 86−91.
(34) Mason, E. A.; McDaniel, E. W. *Transport Properties of Ions in Gases*; Wiley: New York, 1988.

directly. TFA was used as a solvent because the peptides are, at best, marginally soluble in water and methanol. Singly charged ions are dominant in the mass spectra under our experimental conditions.

Molecular Dynamics Simulations. Molecular dynamics (MD) simulations were performed to help interpret the experimental results. The simulations were done with the MACSIMUS suite of programs[35] using the CHARMM21.3 parameter set. A dielectric constant of 1.0 was employed. Cross sections were calculated with MOBCAL,[31] using in most cases the trajectory method (where the long-range interactions between the ion and the buffer gas are accounted for using model potentials).[32] MOBCAL integrates over all possible collision geometries for a given structure, and the calculated cross sections are then usually averaged over 50 structures taken from the last 35 ps of an MD simulation. If the geometry from the simulations is correct, the measured and calculated cross sections are expected to agree to within ±2%.

MD simulations with a classical force field are not suited to study the proton transfer events that are important in these studies, and we are limited to performing simulations for peptides with the proton fixed at particular sites. Since alanine does not have a basic side chain, the most likely protonation sites are the N-terminus amine, the backbone amide CO and NH groups, and the carboxyl CO. Theoretical studies indicate that the carboxyl CO has the lowest proton affinity of these sites (probably around 70−90 kJ mol^{-1} less than that of the N-terminus), and that the amide CO has a proton affinity higher than that of the amide NH.[16,36] A number of recent theoretical studies for Gly_2 and Gly_3 suggest that protonation at the amide CO nearest the N-terminus is almost isoenergetic with protonation at the N-terminus amine.[15,16,37] However, protonation at backbone CO groups further from the N-terminus may not be as favorable.

When protonated at the N-terminus amine, the globule is the lowest energy conformation in the MD simulations for peptides with up to at least 25 residues. Simulations started from a helical conformation rapidly collapse into a globule because locating the proton at the N-terminus leads to unfavorable interactions between the charge and the helix macrodipole. When the proton is located on the carboxyl CO or on the amide CO nearest the C-terminus, the helix is the lowest energy conformation, at least for peptides with 10−25 residues. The helix that results from the MD simulations is in some cases slightly distorted at the C-terminus due to interactions between the protonation site and the dangling carbonyl groups at the C-terminus.

Results

A. Room-Temperature Studies. Figure 2 shows examples of room temperature drift time distributions recorded for $A_{10} + H^+$, $A_{15} + H^+$, $A_{20} + H^+$, $A_{25} + H^+$, and $A_{15}NH_2 + H^+$. Only a single peak is observed for $A_{10} + H^+$, while two peaks are observed for the larger peptides (a third low abundance peak is also present for $A_{20} + H^+$ and $A_{25} + H^+$). These peaks are assigned as follows: the peak for $A_{10} + H^+$ and the dominant peaks for $A_{15} + H^+$, $A_{20} + H^+$, $A_{25} + H^+$, and $A_{15}NH_2 + H^+$ are assigned to a globule; the peak at longer drift times for $A_{15} + H^+$, $A_{20} + H^+$, $A_{25} + H^+$, and $A_{15}NH_2 + H^+$ is due to a helix, and the small peak at short drift times for $A_{20} + H^+$ and $A_{25} + H^+$ is assigned to a helical dimer. The assignments are discussed further below. The measured (room temperature) cross sections for the features assigned to the helix and globule are shown in Table 1. Cross sections calculated for the helix and globule from MD simulations are in good agreement with the measured values. The helix relative abundances (which are reproducible to within around ±3%) increase with peptide size

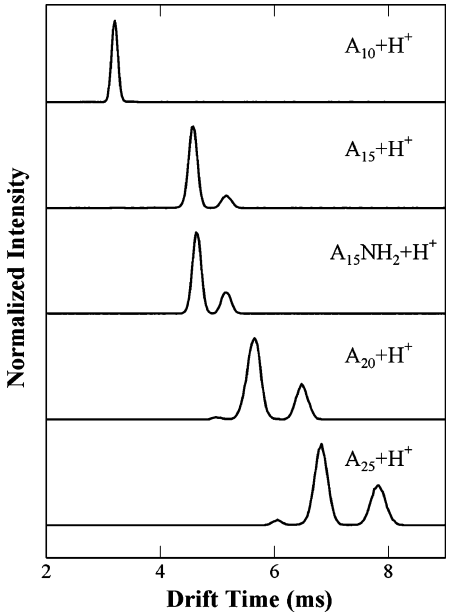

Figure 2. Room temperature drift time distributions for $A_{10} + H^+$, $A_{15} + H^+$, $A_{15}NH_2 + H^+$, $A_{20} + H^+$, and $A_{25} + H^+$. The dominant peak in each case is due to a globule. The second peak at longer drift times for $A_{15} + H^+$, $A_{15}NH_2 + H^+$, $A_{20} + H^+$, and $A_{25} + H^+$ is due to a helix. The small peaks at short drift times for $A_{20} + H^+$ and $A_{25} + H^+$ are assigned to helical dimers. The assignments are discussed in the text. All distributions were recorded with an injection energy of 500 eV.

Table 1. Measured Room Temperature Cross Sections for the Features Assigned to the Helices and Globules

	Room Temperature Cross Section (in Å^2)	
peptide	globule	helix
$A_{10} + H^+$	181	
$A_{15} + H^+$	236	266
$A_{15}NH_2 + H^+$	238	265
$A_{20} + H^+$	292	337
$A_{25} + H^+$	354	407

($A_{15} + H^+$ 14%, $A_{15}NH_2 + H^+$ 23%, $A_{20} + H^+$ 27%, and $A_{25} + H^+$ 36%).

Figure 3 shows a plot of the room temperature drift time distributions for $A_{20} + H^+$ recorded as a function of the injection energy into the drift tube. As the injection energy is lowered, the peak with the smallest drift time (which is assigned to the helical dimer) becomes much more abundant (an injection energy of 500 eV was used to record the data shown in Figure 2). As the ions are injected into the drift tube at elevated kinetic energies, they experience a transient heating and cooling cycle, which at high enough injection energies can lead to dissociation.[38] This evidently occurs for the helical dimer.

Figure 4 shows the final structure from an MD simulation of the $(A_{20} + H^+)_2$ helical dimer. The structure shown in the figure is one of many low-energy helical dimer conformations found in a series of MD simulations initiated from two antiparallel α-helices. Both helices are protonated at the N-terminus amine. The measured cross section for the feature with the shortest drift time in Figure 3 is in good agreement with cross sections calculated for the antiparallel helical dimer conformation represented in Figure 4. The other plausible geometry is a globular dimer. However, low-energy globular dimers have cross

(35) http://www.icpf.cas.cz/jiri/macsimus/default.htm.
(36) Zhang, K.; Cassady, C. J.; Chung-Phillips, A. *J. Am. Chem. Soc.* **1994**, *116*, 11512−11521.
(37) Kohtani, M.; Breaux, G. A.; Jarrold, M. F. *J. Am. Chem. Soc.* **2004**, *126*, 1206−1213.
(38) Jarrold, M. F.; Honea, E. C. *J. Phys. Chem.* **1991**, *95*, 9181−9185.

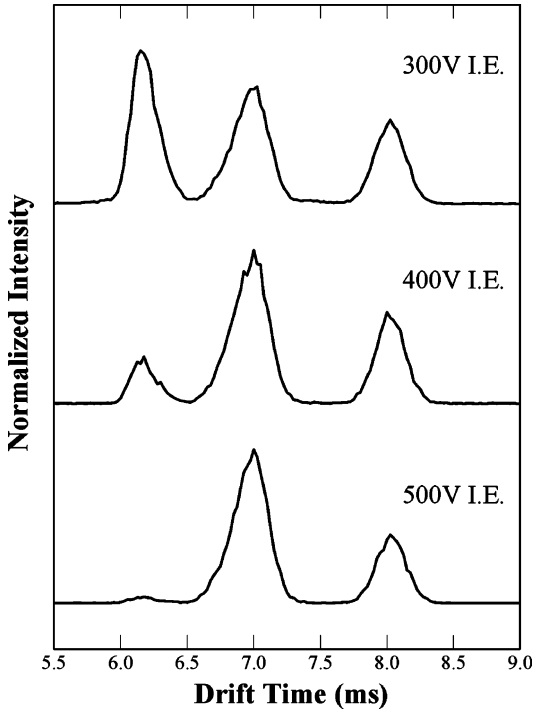

Figure 3. Plot showing the influence of the injection energy on the relative abundances of the peaks observed for $A_{20} + H^+$. The peak at short drift time is due to the $(A_{20} + H^+)_2$ helical dimer. The middle peak is due to an $A_{20} + H^+$ globule. The peak at long drift time is due to an $A_{20} + H^+$ helix.

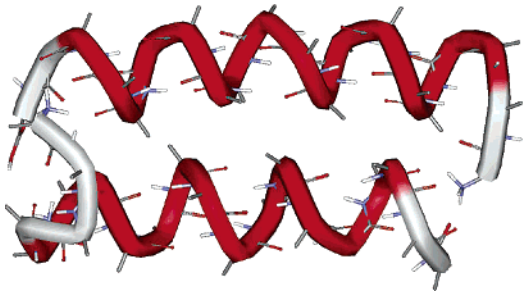

Figure 4. Representative $(A_{20} + H^+)_2$ antiparallel helical dimer conformation obtained from molecular dynamics simulations (see text).

sections that are too small to match the measured value.[39] Note in Figure 4 how the protonated N-terminus of one peptide interacts with the C-terminus of the other. The helices are stabilized by interactions between the charge and the helix macrodipole and by hydrogen bonds between the protonated amine and the dangling CO groups at the C-terminus (helix capping interactions). These helical dimers are very similar to those found previously for $Ac-KA_n + H^+$ peptides.[24]

B. High-Temperature Studies: Collision Cross Sections. Figure 5 shows examples of the drift time distributions recorded for $A_{20} + H^+$ between 373 and 473 K. In this temperature range, the peaks due to the helix and globule merge and are replaced by a single peak that lies between the positions of the helix and globule peaks. The bridge between the peaks evident in the drift time distribution recorded at 433 K results from ions that start at the entrance of the drift tube in one conformation and then convert at some point along the length of the drift tube into the other. Thus, the ion spends part of its time in each form, and so it has a drift time between those of the two

(39) Hudgins, R. R.; Kinnear, B. S.; Jarrold, M. F. Unpublished data.

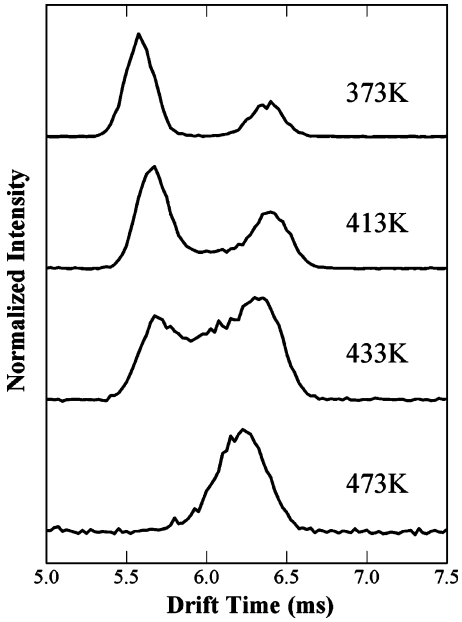

Figure 5. Drift time distributions recorded for $A_{20} + H^+$ as a function of temperature. The larger peak on the left at 373 K is due to the globule, while the smaller peak on the right is due to the helix.

conformations. At 433 K, the time scale for interconversion between the two conformations is comparable to the drift time. At higher temperatures, the rate of the helix/globule transitions increases, so that the time scale for interconversion becomes much less than the drift time. Conformational averaging then yields the narrow peak evident at 473 K in Figure 5. Note that this peak lies closer to the position of the helix peak than to the globule. This indicates that at 473 K, $A_{20} + H^+$ spends more time in the helical conformation than as a globule. This is an apparent reversal of the situation at 373 K, where the globule peak is more abundant than the helix peak. However, at 373 K, the helix and globule are not freely interconverting on the experimental time scale (the conformations are not in equilibrium), and the measured relative abundance may not reflect the equilibrium populations at 373 K.

Relative cross sections for $A_{20} + H^+$ and the other peptides studied here are plotted in Figure 6. The relative cross sections are obtained by subtracting the smallest cross section measured for the globular conformation of each peptide from the measured or calculated cross sections. A large positive deviation of the relative cross section from zero indicates a molecular structure distinctly less compact than the globule. When two isomers interconvert, as discussed above for $A_{20} + H^+$, an intensity-averaged cross section was calculated from

$$\bar{\sigma} = \frac{\sum I(t) \times \sigma(t)}{\sum I(t)} \qquad (2)$$

where $I(t)$ is the signal intensity at drift time t, and $\sigma(t)$ is the cross section at drift time t. The dashed lines in Figure 6 show cross sections calculated as a function of temperature for the final structures taken from the lowest energy room temperature MD simulations for $A_{15} + H^+$, $A_{20} + H^+$, and $A_{25} + H^+$, protonated at the C-terminus. The final structures are all helical, and so these results show how the cross sections for the helices should behave as a function of temperature if there are no

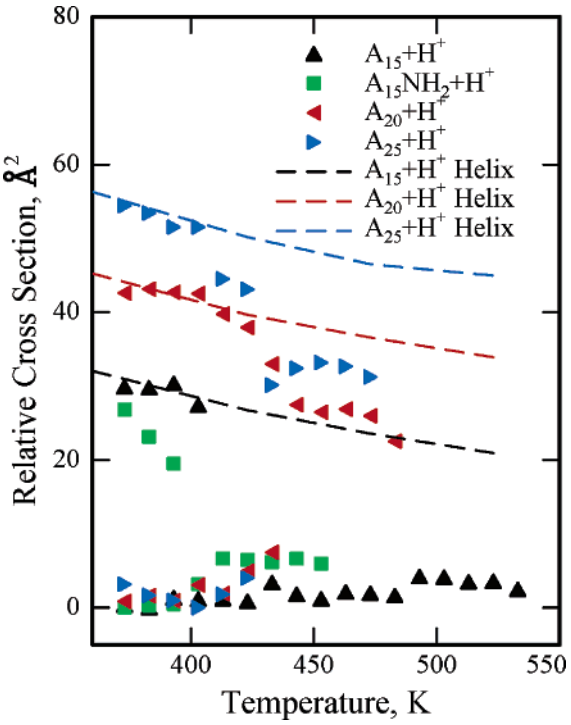

Figure 6. Plot of the relative collision cross sections of polyalanine peptide ions ($A_{15} + H^+$, $A_{15}NH_2 + H^+$, $A_{20} + H^+$, and $A_{25}+H^+$) against drift tube temperature. The relative cross sections are obtained by subtracting the smallest cross section measured for the globular conformation of each peptide from the measured or calculated cross sections (see text). All measurements were performed with an injection energy of 500 eV. At high temperatures, where the helix and globule interconvert rapidly on the experimental time scale, the intensity-averaged cross section is plotted (see text). The dashed lines show calculated cross sections for rigid $A_n + H^+$ helices.

structural changes. The calculated cross sections systematically decrease because the long-range interactions become less important as the temperature is increased, and the collisions become harder and ride further up the repulsive walls. Below the transition temperatures, the measured cross sections for the $A_{15} + H^+$, $A_{20} + H^+$, and $A_{25} + H^+$ helices track the calculated cross sections (dashed lines in Figure 6).

For $A_{10} + H^+$, only a single peak, assigned to a globule, is observed at room temperature, and this conformation persists to the highest temperature studied. Since only the globule is observed for $A_{10} + H^+$, results for this peptide are not shown in Figure 6. For $A_{15} + H^+$, the helix and globule peaks merge between 373 and 443 K. The merged peak has a cross section that is almost identical to the extrapolated value for the globule. In other words, the $A_{15} + H^+$ helix converts almost completely into the globule as the temperature is increased. The behavior of $A_{15}NH_2 + H^+$ is similar to that of $A_{15} + H^+$, except that the transition occurs at a slightly (~10 K) lower temperature, and the merged peak is slightly, but significantly, larger than the extrapolated value for the globule. For $A_{20} + H^+$ and $A_{25} + H^+$, the cross sections after the transition lie closer to the helix than to the globule, indicating that at high temperatures, these peptides spend more time in the helical conformation than in the globule. The position of peaks indicates that the fraction of the time spent in the helical conformation is around 70% for both peptides. The fraction is slightly larger for $A_{20} + H^+$ than for $A_{25} + H^+$, but the difference is small and may not be significant.

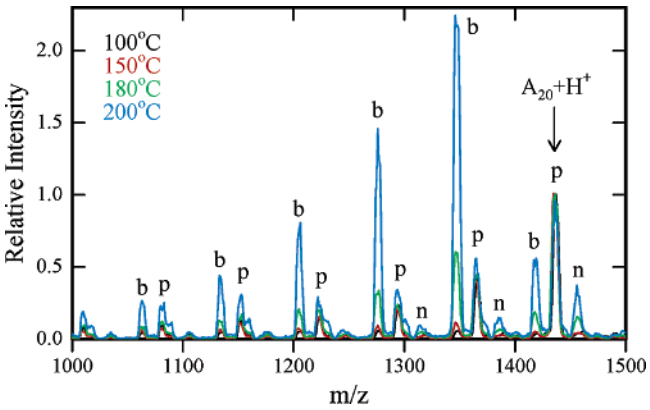

Figure 7. Mass spectra recorded for the A_{20} peptide as a function of drift tube temperature. The intensities in each spectrum have been normalized so that the relative intensity of the $A_{20} + H^+$ peak is 1.0. The peaks labeled p are the $A_n + H^+$, $A_{n-1} + H^+$, $A_{n-2} + H^+$, ... series that include A_{20} and the deletion byproducts (see text). The peaks labeled b are due to the b series of fragment ions ($A_n-H_2O + H^+$, $A_{n-1}-H_2O + H^+$, $A_{n-2}-H_2O + H^+$, ...). The peaks labeled n are due to the sodiated series ($A_n + Na^+$, $A_{n-1} + Na^+$, $A_{n-2} + Na^+$, ...).

C. High-Temperature Studies: Peptide Fragmentation. As the temperature is increased, the peptides eventually fragment. Analysis of the fragmentation behavior is complicated by the fact that the protonated peptide ions are not mass selected before they enter the drift tube. Thus, in addition to the protonated $A_n + H^+$ peptide ions, there are deletion peptides ($A_{n-1} + H^+$, $A_{n-2} + H^+$, ...) that are byproducts of the peptide synthesis and sodiated peptides ($A_n + Na^+$, $A_{n-1} + Na^+$, $A_{n-2} + Na^+$, ...) that are often formed by electrospray. However, it is still possible to identify the dominant fragmentation pathways. Figure 7 shows mass spectra recorded for the A_{20} peptide as a function of drift tube temperature. The intensities in each spectrum have been normalized so that the relative intensity of the $A_{20} + H^+$ peak is 1.0. The peaks labeled p in Figure 7 are the $A_n + H^+$, $A_{n-1} + H^+$, $A_{n-2} + H^+$, ... series that include A_{20} and the deletion byproducts, and the peaks labeled n are due to the sodiated series ($A_n + Na^+$, $A_{n-1} + Na^+$, $A_{N-2}+Na^+$, ...). The relative intensities of the sodiated ions increase as the temperature is increased. This occurs because the sodiated ions are more stable than the protonated ones and dissociate at a higher temperatures. The peaks labeled b in Figure 7 are due to the b series of fragment ions ($A_n-H_2O + H^+$, $A_{n-1}-H_2O + H^+$, $A_{n-2}-H_2O + H^+$, ...). For the $A_n + H^+$ peptide ions, the dominant fragment is the b_{n-1}^+ ion ($A_{n-1}-H_2O + H^+$), while for $A_{15}NH_2 + H^+$, the dominant fragment is the b_n^+ ion ($A_n-NH_3 + H^+$). As the temperature is increased, more extensive fragmentation occurs, and the abundances of the smaller fragments increase at the expense of the larger ones. Because of the long time scale and the relatively gentle heating of the ions, it is reasonable to assume that we observe the lowest energy fragmentation pathways in these studies. Similar fragments have been observed in collision-induced dissociation and metastable dissociation studies of smaller peptides.[40,41]

Table 2 summarizes the fragmentation efficiencies, determined by dividing the sum of the intensities of the dominant

(40) Yalcin, T.; Knouw, C.; Csizmadia, I. G.; Peterson, M. R.; Harrison, A. G. *J. Am. Soc. Mass Spectrom.* **1995**, *6*, 1164−1174.
(41) Yalcin, T.; Csizmadia, I. G.; Peterson, M. R.; Harrison, A. G. *J. Am. Soc. Mass Spectrom.* **1996**, *7*, 233−242.

Table 2. Fragmentation Efficiencies (Calculated by Dividing the Sum of the Intensities of the Dominant Fragments by the Sum of $A_n + H^+$ Intensities)[a]

	Fragmentation Efficiency (at 473 K)	
peptide	300 eV IE	500 eV IE
$A_{10} + H^+$	<0.1	0.2
$A_{15} + H^+$	0.2	0.4
$A_{15}NH_2 + H^+$	4.4	7.3
$A_{20} + H^+$	0.9	1.8
$A_{25} + H^+$	1.0	4.0

[a] The results were obtained with a drift tube temperature of 473 K and with injection energies (IE) of 300 and 500 eV.

fragments by the sum of $A_n + H^+$ intensities. The results shown in the table were obtained with a drift tube temperature of 473 K and with injection energies of 300 and 500 eV. The injection energy influences the amount of fragmentation that occurs at intermediate drift tube temperatures but has less effect at high and low temperatures. At room temperature, with an injection energy of 500 eV (the maximum employed here), fragmentation is not observed (except for the dimer). Hence, the drift tube temperature must be elevated for the peptides to fragment; injection energies of up to 500 eV contribute to fragmentation, but fragmentation results primarily from the effects of the elevated drift tube temperature. $A_{15}NH_2$ has the largest fragmentation efficiency in Table 2. For the A_n peptides, the fragmentation efficiencies increase as n increases.

Discussion

A. Globules and Helices at Room Temperature. The conformations of unsolvated polyalanine peptide ions, $A_n + H^+$ ($n = 3-20$), have previously been studied by our group using high-resolution ion mobility measurements.[19] The globule and dimer were observed in those studies, but the helical conformation was not found. The cross sections of the peaks assigned to the globule in the present work are in excellent agreement with the cross sections measured previously (root mean square deviation <0.5%). The cross sections recorded for the $A_n + H^+$ features assigned here to the helix are within 1% of the cross sections measured for $A_n + Na^+$ helices.[26] The effect of substituting Na^+ for H^+ on the overall cross section for such a large system is expected to be small.

The principle difference between the measurements reported here and the previous high-resolution ion mobility study (where helices were not observed) is in the way the ions are transferred to the drift tube.[19] The high-resolution ion mobility measurements are performed at atmospheric pressure, and the electrosprayed ions are transferred from the source to the drift tube through an ion gate.[42] The ion gate uses electric fields to drag the ions into the drift tube against a counter flow of helium buffer gas that prevents the air and solvent from entering. This is a gentle interface where the ions are not significantly heated. In the present experiment, the ions are admitted into the apparatus through a heated capillary interface, and then after passing through a differentially pumped region, they are accelerated and injected into the drift tube at elevated kinetic energies. The injection energy is required to overcome the buffer gas flow out of the drift tube.

The polyalanine peptides are not expected to be helical in the TFA/water mixture used to dissolve the peptides for electrospray. Thus, the absence of the helix in the high-resolution ion mobility measurements presumably results because the ions are not heated in the interface region, so the observed conformations reflect the structures present in solution. In the experiments reported here, thermal heating in the capillary interface and collisional heating as the ions enter the drift tube can drive conformational changes, so that the conformations observed are those that are stable in the gas phase. The helical dimer is also observed in the high-resolution ion mobility measurements. However, this is not proof that the dimer is present in solution. We consider it more likely that the dimer forms during the electrospray process, as the ions are evolving from the evaporating droplets. It is worth noting that formation of the helical dimer from two globular monomers (from solution) requires substantial conformational changes. The globule to helix transition apparently occurs more readily in the dimer than in the monomer. This may be because the charge can remain at the N-terminus (the preferred protonation site in solution) in the dimer, but it must relocate to the C-terminus during a globule to helix transition in the monomer.

For $A_{20} + H^+$ and $A_{25} + H^+$, it is evident that the helix and the globule have similar stabilities in the gas phase and that the helix can be generated by heating the globule. For $A_{15} + H^+$, however, the helix which is observed at room temperature disappears as the temperature is increased. The helix is evidently less stable than the globule for $A_{15} + H^+$, and since the helix is not present in solution, there is obviously a question about the origin of the helix observed at room temperature. The most plausible explanation is that it results from dissociation of a dimer. In the dimer, we assume that the individual peptides are protonated at their N-terminus amine, and that the protonated amine of one peptide folds over and interacts with the C-terminus of the other (see Figure 4). When the helical dimer dissociates, the charge may either stay with the N-terminus amine or transfer to the C-terminus of the other peptide. If the proton transfers to the C-terminus, it retains its favorable interactions with the helix macrodipole and so the peptide will stay helical as the dimer dissociates, but if the proton remains on the N-terminus amine as the dimer dissociates, the separated helix will rapidly collapse to a globule because a positive charge at the N-terminus interacts unfavorably with the helix macrodipole (see above). Thus, dissociation of the dimer could lead to both helical and globular products depending on the extent of proton transfer during the dissociation process.

B. Interconversion between Globules and Helices. Our previous studies have shown that helix formation in unsolvated peptides with nonpolar side chains is driven by the location of the charge through its interactions with the helix macrodipole.[19,23−28,43] The acetylated analogues of the polyalanine peptides studied here ($Ac-A_n + H^+$) are all helical.[26] In these peptides, the acetyl group blocks the N-terminus, so that the only protonation sites available are on the backbone. Protonation near the C-terminus is favorable for these peptides because they can then adopt a helical conformation which is lower in energy (according to MD simulations) than the globular conformations that result from protonation near the N-terminus. Protonation near the middle of the peptide is expected to lead to partially helical structures, where the peptide is helical from the N-terminus to the protonation site and then globular to the C-terminus.

(42) Dugourd, Ph.; Hudgins, R. R.; Clemmer, D. E.; Jarrold, M. F. *Rev. Sci. Instrum.* **1997**, *68*, 1122−1129.

(43) Kohtani, M.; Jarrold, M. F. *J. Am. Chem. Soc.* **2002**, *124*, 11148−11158.

Structures such as this have been found in MD simulations, but they have not been observed experimentally, suggesting that there is a strong driving force to locate the proton at the C-terminus and maximize the number of helical residues. Incorporation of a basic residue at the N-terminus as, for example, in $Ac-KA_n + H^+$, leads to a globular conformation. Here, the basic residue pins the proton at the N-terminus so that it cannot migrate to the C-terminus. In the peptides studied here, it is evident that the N-terminus amine is able to pin the charge at the N-terminus for $A_{10} + H^+$ ($A_{10} + H^+$ is a globule-like $Ac-KA_{10} + H^+$, while $Ac-A_{10} + H^+$ with a blocked N-terminus is a helix). This is consistent with surface-induced dissociation studies which suggest that in peptides without basic residues, the N-terminus amine sequesters the proton.[7] On the other hand, for $A_{15} + H^+$, $A_{20} + H^+$, and $A_{25} + H^+$, both the helix and the globule are observed. The energy gained by converting a globule to a helix (both protonated near their C-termini) is expected to increase as the peptide becomes longer.[44] So, for a larger peptide, the energy gained by converting the globule to a helix can overcome the difference between the proton affinities of the N-terminus amine and the backbone carbonyl groups near the C-terminus. A globule protonated at the N-terminus amine and a helix protonated near the C-terminus then have comparable energies. At room temperature, the rate of interconversion between these two states is small, and separate well-resolved peaks are observed in the drift time distributions. As the temperature is increased, the time scale for interconversion becomes comparable to the drift time, and the peaks broaden and eventually merge.

C. The Mobile Proton. The conformational changes outlined above are driven by proton transfer, and hence the rates of the conformational changes provide a measure of the rate of proton transfer. The results in Figure 5 indicate that proton transfer becomes fast on the millisecond time scale of the ion mobility measurements at around 450 K for $A_{20} + H^+$. Proton transfer, here, is between the two preferred protonation sites at the ends of the peptide. Proton transfer between these sites probably involves a number of intermediate steps where the proton is transferred from one backbone carbonyl to another. This transfer is expected to be facile, except that it may be slowed by self-solvation where the protonation site becomes surrounded by a shell of backbone carbonyl groups. It is likely that helix formation will follow proton transfer; thus, we envision proton transfer from the N- to the C-terminus as occurring through a series of steps, with a helix at the N-terminus side of the proton and a globular conformation on the C-terminus side. On average, the charge is expected to "pool" at the most-favorable protonation sites, which is at the ends of the peptide.

(44) Kohtani, M.; Jarrold, M. F. *J. Am. Chem. Soc.* **2004**, *126*, 8454−8458.

Several different mechanisms have been proposed to account for the formation of the b_n^+, b_{n-1}^+, b_{n-2}^+, b_{n-3}^+, ... series of fragment ions.[15,41] There is agreement that for formation of the dominant fragment ions (b_n^+ for $A_{15}NH_2 + H^+$ and b_{n-1}^+ for $A_{10} + H^+$, $A_{15} + H^+$, $A_{20} + H^+$, and $A_{25} + H^+$), the charge must be located at or near the C-terminus. There is clearly a correlation between the ease of fragmentation and the tendency to form a helical conformation for the $A_{10} + H^+$, $A_{15} + H^+$, $A_{20} + H^+$, and $A_{25} + H^+$ peptides. Formation of a stable helix requires protonation at the C-terminus, and protonation at the C-terminus is required for dissociation to the b_n^+, b_{n-1}^+, b_{n-2}^+, b_{n-3}^+, ... series of fragment ions. So, helix formation promotes dissociation because it pools the proton at the C-terminus. Peptides with basic residues, such as $Ac-KA_{15} + H^+$, fragment at even higher temperatures than do the polyalanine peptides. This observation is in agreement with the shift to a higher threshold energy for collision-induced dissociation that is observed for peptides with localized charges.[6]

Conclusions

High-temperature ion mobility measurements have been used to probe the conformations of protonated polyalanine peptides ($A_{10} + H^+$, $A_{15} + H^+$, $A_{20} + H^+$, $A_{25} + H^+$, and $A_{15}NH_2 + H^+$) from room temperature up to the point where they dissociate. A globule and helix coexist at room temperature for all peptides but $A_{10} + H^+$. As the temperature is increased, they interconvert, and the peaks assigned to the globule and helix broaden and merge to give a single narrow peak. Since these conformational changes are driven by proton transfer, our results suggest that the proton becomes mobile (able to migrate along the backbone) at around 450 K in these peptides. For $A_{15} + H^+$ and $A_{15}NH_2 + H^+$, the merged peak is close to the expected position for the globular conformation, indicating that these peptides spend most of their time as globules when heated. The location of the merged peaks for $A_{20} + H^+$ and $A_{25} + H^+$ suggests that these peptides spend around 70% of their time in the helical conformation, up to the point where they dissociate. There is a correlation between the time spent in the helical conformation and the ease of dissociation. The helical conformation pools the proton at the C-terminus, which is required for dissociation to give the observed b_n^+, b_{n-1}^+, b_{n-2}^+, b_{n-3}^+, ... series of fragment ions.

Acknowledgment. We gratefully acknowledge the support of the National Institutes of Health and the National Science Foundation. J.E.S. was supported through an NSF REU program at Indiana University.

JA045336D